Modeling discontinuous gas flow for remediation in heterogeneous media

Paul R. Hegele, Kevin G. Mumford
Department of Civil Engineering – Queen's University, Kingston, Ontario, Canada

2011 Pan-Am CGS Geotechnical Conference

ABSTRACT
During the remediation of contaminated soils and groundwater, gases can be trapped in the subsurface. When injected or produced at slow rates in coarse saturated media, discontinuous (bubbly) gas flow can occur, which is characterized by disconnected gas clusters which can fragment, mobilize and coalesce during buoyancy-driven migration. It is thought that discontinuous gas flow is advantageous during remediation because it has a higher gas-liquid interfacial area than continuous channels, thereby maximizing mass transfer in or out of the gas phase and increasing remediation efficiency. However, heterogeneities can cause pooling and lateral spreading of the gas, affecting its distribution and availability for mass transfer. In this study, a macroscopic invasion percolation model was used to simulate discontinuous gas flow in the presence of heterogeneities. It was found that heterogeneities can decrease relative mass transfer rates under conditions of slower flow, but can increase relative mass transfer rates under conditions of faster flow.

RÉSUMÉ
Pendant la décontamination d'un sol et de l'eau souterraine, il est possible que des gaz soient emprisonnés sous la surface. Lorsqu'injectée ou produit à faible taux dans un média saturé grossier, un flot discontinu (bulle) de gaz se produit, lequel est caractérisé par des grappes de gaz discontinues pouvant se fragmenter, se mobiliser ou s'agglutiner alors qu'ils entreprennent une migration dû à leur flottaison. Il est pensé qu'un flot discontinu de gaz est avantageux durant la réhabilitation d'un sol parce qu'il possède une plus grande aire à l'interface gaz-liquide qu'un flot continu. Ainsi, un transfère de masse est maximal entrant ou sortant de la phase gazeuse augmentant ainsi l'efficacité de réhabilitation. Cependant, l'hétérogénéité du sol peut causer des accumulations ou un écoulement latéral du gaz affectant ainsi sa subséquente distribution et sa disponibilité pour le transfère de masse. Dans cette étude, un modèle d'invasion par percolation macroscopique fut utilisé pour simuler l'écoulement d'un flot gazeux discontinu dans un milieu poreux saturé. Il fut trouvé qu'avec un faible flot, les hétérogénéités peuvent réduire le taux relatif du transfert de masse et qu'avec un important flot, les hétérogénéités peuvent accroître le taux relatif du transfert de masse.

1 INTRODUCTION

Nonaqueous phase liquids (NAPLs) and other contaminants in the subsurface can pose long term threats to human and ecological health. The presence of these contaminants at brownfield sites can also impede their redevelopment. As such, remediation techniques need to be continually developed, evaluated and refined to ensure rapid and economic site remediation.

Many remediation technologies can produce gases in the subsurface while treating contaminated soil and groundwater. These can be produced as a result of direct injection (e.g., in in-situ air sparging and biostimulation applications), as a result of chemical reactions (e.g., due to chemical oxidation and biodegradation processes), or as a result of heat-induced phase transitions (e.g., during in-situ thermal remediation). When injected or produced at slow rates in coarse media, the gas flow can be discontinuous, which is characterized by disconnected clusters or bubbles undergoing buoyancy-driven migration. At faster rates in fine media, continuous gas flow can occur, which is characterized by stable channels or fingers (e.g., Geistlinger et al. 2006). Gases undergoing discontinuous flow have a higher interfacial area per unit volume than those undergoing continuous flow, yielding higher mass transfer rates between the gas and aqueous phases. As such, it is important to understand the type of gas flow that is occurring during the application of the aforementioned remediation techniques, whose processes often depend on the mass transfer between the gas and aqueous phase.

The purpose of this study is to describe and quantify the potential effects of heterogeneity on discontinuous gas flow distributions using a numerical model. By approximating interfacial area and relative permeability based on the simulated gas distributions, inferences will be made into how heterogeneities can affect mass transfer rates during remedial applications. A previously developed macroscopic invasion percolation model (Mumford et al. 2010) was first validated against experimentally-derived saturation fields in homogeneous silica sands. The model was then applied in simple heterogeneous systems. The findings presented herein provide a better understanding of the effects of layered heterogeneities on discontinuous gas flow patterns, relative permeability, gas-liquid interfacial area and mass transfer by comparing different heterogeneous simulations to a reference homogeneous simulation.

2 BACKGROUND AND MODEL DESCRIPTION

A macroscopic invasion percolation model was used to simulate discontinuous gas flow through saturated porous

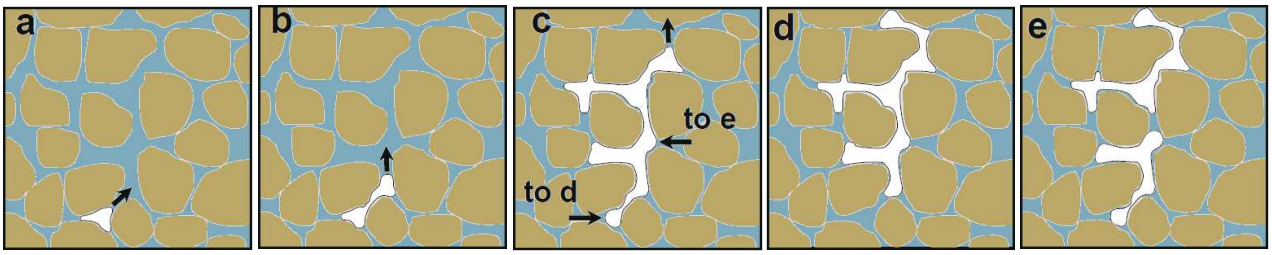

Figure 1: Adapted from Mumford et al. (2009). (a) An initial gas cluster (b) invades the lowest adjacent entry threshold and (c) migrates vertically due to hydrostatic pressures. If the condition for wetting fluid reinvasion is met, (d) mobilization or (e) fragmentation of the gas cluster may occur, depending on where the wetting fluid reinvades the gas.

media in both homogeneous and heterogeneous systems. This model includes a gravity gradient, as well as fragmentation and mobilization mechanisms as the gas clusters migrate upwards. The model assumes capillary-dominated conditions, typical of gas cluster migration under very slow flow rates where viscous forces are considered negligible (e.g., Geistlinger et al. 2006).

2.1 Discontinuous Gas Flow Mechanisms

The two main types of gas flow through saturated porous media which have been observed experimentally are continuous and discontinuous flow (e.g., Brooks et al. 1999; Stöhr and Khalili 2006; Geistlinger et al. 2006). Continuous flow, also known as coherent or channelled flow, is characterized by stable channels or fingers, whereas discontinuous flow is characterized by disconnected gas clusters (i.e., bubbles) that can fragment, mobilize and coalesce. Gas flow transitions from discontinuous to continuous as flow rates increase above a critical flow rate (Q_{crit}):

$$Q_{crit} = \frac{\pi \Delta\rho g {r_c}^4}{8\mu_g} \quad [1]$$

where $\Delta\rho$ is the density difference between the fluids, g is the gravitational constant, r_c is the characteristic capillary radius and μ_g is the dynamic viscosity of gas (Geistlinger et al. 2006). At slow rates, the migration of the gas is dominated by buoyancy and capillary forces, and viscous forces are negligible. Equation 1 shows that the critical flow rate is highly dependent on the gas's characteristic capillary radius, which is proportional to the grain size of the media through which the gas is flowing. As such, gas flow is usually discontinuous in coarser media; this has been demonstrated by numerous studies (e.g., Reddy et al. 2001; Geistlinger et al. 2006; Mumford et al. 2009). However, discontinuous flow can occur in finer media if injection rates are small enough (Mumford et al. 2009).

As discontinuous gas clusters or fingers migrate vertically, they can undergo fragmentation and mobilization, as shown in Figure 1a-e. These processes are largely dependent on local pore throat entry pressures for the wetting and nonwetting phases (water and gas, respectively, in cases considered here), as well as the hydrostatic gradient in the system. It should be noted that these fragmentation processes can sometimes lead to trapping of the wetting phase between two gas-filled pore bodies (as shown in Figure 1e). This can cause injected gas to circumvent these trapped throats, creating lateral migration paths and conical distributions (Stöhr and Khalili 2006). This circumventing behaviour is referred to as branching, and is not considered in this study.

2.2 Discontinuous Gas, Mass Transfer and Remediation

Remediation technologies that inject air into the subsurface or rely on degassing (Zhao and Ioannidis 2011) are designed to exploit the mass transfer between the injected gas phase and the aqueous phase to remediate the contaminant. This mass transfer can be either in to or out of the gas phase. For example, in-situ air sparging works by injecting air to volatilize contaminants for subsequent removal by soil vapour extraction (SVE) systems (Johnson et al. 1993). Air or oxygen can also be injected to enhance and control aerobic biodegradation during biostimulation applications (Geistlinger et al. 2005). As such, it is important to understand the relationship between mass transfer and the distribution of the injected gas.

The solute mass transfer flux (S) of a compound between the gas and aqueous phase can be expressed as:

$$S = k_f \alpha (C_s - C) \quad [2]$$

where α is the interfacial area between the phases, C is the aqueous concentration of the compound, C_s is the aqueous solubility of the compound and k_f is the mass transfer coefficient (e.g., Powers et al. 1994). Neglecting dispersion, Equation 2 can be combined with the one dimensional advection equation (i.e., neglecting dispersion) to yield:

$$\frac{\partial C}{\partial t} = -q\frac{\partial C}{\partial x} + k_f \alpha (C_s - C) \quad [3]$$

where $\partial C/\partial t$ is the change in aqueous concentration over time, q is the Darcy flux, and $\partial C/\partial x$ is the change in aqueous concentration over a characteristic length L (e.g., Powers et al. 1992). At steady state, for a boundary condition of $C = 0$ at $x = 0$ (Powers et al. 1992):

$$J = qC_s\left[1 - \exp\left(\frac{-k_f \alpha L}{q}\right)\right] \quad [4]$$

where J is the aqueous mass flux at L. By expressing the Darcy flux in terms of the relative wetting permeability, Equation 4 becomes:

$$J = \left(\frac{k_{rw} k \rho_w g}{\mu_w} \nabla h\right) C_s \left[1 - \exp\left(\frac{-k_f \alpha L \mu_w}{k_{rw} k \rho_w g \nabla h}\right)\right] \quad [5]$$

where k_{rw} is the relative wetting permeability, k is the intrinsic permeability, ρ_w is the density of water, μ_w is the dynamic viscosity of the water, and ∇h is the hydraulic gradient.

Equation 5 shows that the mass flux is dependent on both the interfacial area and relative wetting permeability. When gas flow is discontinuous, the gas-liquid interfacial area is expected to be larger than in continuous systems, thereby maximizing mass transfer and increasing remediation efficiency. This is one reason why pulsed injection during air sparging has been shown to maximize contaminant recovery (e.g., Johnson et al. 1999). However, potential decreases in relative wetting permeability must also be considered when evaluating mass transfer between an injected gas and the surrounding aqueous phase.

2.3 Heterogeneity and Discontinuous Gas Flow

Macroscopic heterogeneities have been shown to significantly alter the flow path of buoyancy-driven gas migration both at the laboratory scale (Glass et al. 2000) and the field scale (Tomlinson et al. 2003). Lateral spreading or trapping of the gas can occur if it impacts and migrates along lenses of lower permeability (i.e., capillary barriers). This lateral spreading can increase the radius of influence of sparging zones, but can also cause the gas to bypass contaminants which may be trapped in lenses of lower permeability (Tomlinson et al. 2003). Accumulation of the discontinuous gas behind capillary barriers can also affect remediation efficacy. These accumulations can cause decreases in gas-liquid interfacial area and relative permeability if the pool becomes continuous, thus limiting mass transfer rates in regions where this pooling is observed. For example, Ye et al. (2009) observed significant permeability reductions in regions of pooled methane gas generated by anaerobic biodegradation.

It may be possible to design gas injection systems to minimize the detrimental effects of large-scale heterogeneities at contaminated sites. Since gas flow is more likely to be discontinuous in coarse media, Continuous gas injection into finer media beneath a coarser contaminated layer can cause gas channels to break up and become discontinuous as they enter the coarser layer, thereby increasing interfacial area and mass transfer between aqueous and gas phases (Reddy et al. 2001; Geistlinger et al. 2009).

2.4 Macroscopic Invasion Percolation Model

A two dimensional macroscopic invasion percolation (macro-IP) model was used to simulate discontinuous gas flow through saturated porous media. In traditional invasion percolation (IP), a “ball-and-stick” model is used to represent pore bodies and throats. In contrast, macro-IP uses a lattice of blocks to represent the average behaviour over the pore bodies and throats in each block, thereby allowing a single block to be occupied by two fluids simultaneously (Kueper and McWhorter 1992). IP and macro-IP have been previously modified to include gravity (Ioannidis et al. 1996), fragmentation/mobilization processes (Zhao and Ioannidis 2011; Wagner et al. 1997; Glass and Yarrington 2003), and mass transfer between fluid phases (Mumford et al. 2010). The model used in this study is that of Mumford et al. (2010) neglecting the mass transfer processes.

To simulate discontinuous gas flow, each porous medium was represented by an uncorrelated random distribution of pore radii, based on experimentally-measured capillary pressure-saturation curves (Schroth et al. 1996). Entry and withdrawal thresholds (for gas invasion and water reinvasion, respectively) for each block were assigned based on the radii using the Young-Laplace equation and the hydrostatic pressure at that block. Simulation of gas flow proceeded based on an algorithm where the block with the lowest entry threshold that is neighbouring the injected gas is invaded. The condition for fragmentation and mobilization of the gas clusters, which is characterized by wetting fluid reinvasion, is as follows:

$$P_{t_j} \geq P_{e_i} + \Delta\rho g(z_{i-j}) \quad [6]$$

where P_{e_i} and P_{t_i} are the entry and terminal pressures, and $\Delta\rho g(z_{i-j})$ is the difference in hydrostatic pressure between the i^{th} and j^{th} sites of the gas cluster (Glass and Yarrington 2003). Once additional fragmentation or mobilization ceases, a new invasion event occurs. Simulations were terminated when the gas impacted the top of the domain. This model does not consider the facilitation of wetting phase reinvasion by neighbour site occupancy (Li and Wardlaw 1986), which may overestimate fragmentation and interfacial area (Glass and Yarrington 2003).

2.5 Model Validation

The macro-IP model was validated using fifteen gas injection experiments conducted by Mumford et al. (2009). In these experiments, air was slowly injected (1 µL/min or 10 µL/min) from a point source into 91 mm x 73 mm x 7.9 mm water saturated sand packs to create discontinuous gas clusters (Mumford et al. 2009). The experiments occurred in translucent, homogeneous 12/20, 20/30, and 30/40 (median grain diameters of 1.1 mm, 0.7 mm and 0.5 mm) silica sand (Accusand). The sand packs were created by continuously pouring wet sand into a water-filled glass cell, which resulted in a bulk density of 1.67-1.72 g/cm^3. In each experiment, a light source was placed behind the cell, and digital images were obtained at constant time intervals until 1 mL of gas was injected into the system. To validate the model used in this study, thickness-averaged gas saturation fields were generated from the collected images using a volume-calibrated light transmission method (LTM) modified from Niemet and Selker (2001).

Experimental gas saturation fields derived from the digital images were compared to a Monte Carlo suite of macro-IP simulations. Average values (based on 400 simulations) of the gas saturation, cluster height, maximum cluster width, center of mass and radius of gyration were compared to the experiments at the different grid sizes. Grid sizes between 1 x 1 mm^2 and 2 x 2 mm^2 produced simulations that compared well to the spatial metrics and saturations found in the experiments. An example of a processed experimental image and a simulation with similar metrics is shown in Figure 2. To match the experimental results, the gas saturation in each of the gas-occupied grid blocks was taken to be 0.17 (when simulating 1.1 mm sand at a grid size of 2 x 2 mm^2).

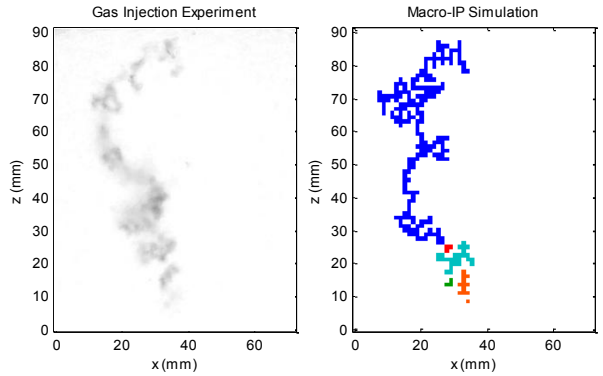

Figure 2: (Left) A saturation field in 1.1 mm silica sand using the volume-calibrated LTM, where black represents a gas saturation of 100% and white represents a gas saturation of 0%. (Right) A macro-IP simulation in 1.1mm silica sand with similar spatial metrics to the experimentally-derived saturation field. The different shades in the macro-IP simulation represent separate, disconnected gas clusters.

3 HETEROGENEOUS SIMULATION APPROACH

3.1 Simulation Conditions

To study the effects of heterogeneity on discontinuous gas flow, five scenarios were investigated:

A. Homogeneous 1.1 mm sand
B. Unbroken 0.7 mm sand barriers in 1.1 mm sand
C. Unbroken 0.5 mm sand barriers in 1.1 mm sand
D. Broken 0.7 mm sand barriers in 1.1 mm sand
E. Broken 0.5 mm sand barriers in 1.1 mm sand

Figure 3 shows the simulation domain. The unbroken and broken simulations were investigated to observe discontinuous gas following breakthrough and lateral spreading, respectively, while the homogeneous simulation was run to provide a reference for comparison.

In each of the scenarios, the dimensions of the system were 1000 mm vertically and 100 mm longitudinally, and the initial injection point was at the very bottom and middle of the domain. The model was run at a validated grid size of 2 x 2 mm^2. The capillary barriers were 20 mm thick, and simulations were run for each scenario with capillary barriers spaced at 135 mm, 185 mm and 235 mm intervals. The areas in between capillary barriers are referred to as “1.1 mm sand compartments”. The input parameters and sand properties for the simulations are given in Table 1. For broken capillary barriers, the break was 10 mm wide at alternating ends of the finer sand lens.

Table 1: Sand properties used in the macro-IP simulations

Media	1.1 mm sand	0.7 mm sand	0.5 mm sand
Particle Diameter[1], d_{50} (mm)	1.105	0.713	0.532
Size Fraction[1]	12/20	20/30	30/40
Porosity[1]	0.348	0.348	0.348
Irreducible Water Saturation[1], S_{wr}	0.035	0.046	0.052
Air entry pressure[1], h_d (mm of water)	54.2	86.6	130.3
Brooks-Corey Pore Size Distribution Index[1], λ	3.94	5.57	6.91
P_e/P_t ratio[2]	1.67	1.20	1.75

[1]Schroth et al. (1996)
[2]Mumford et al. (2009)

3.2 Rate Limited Mass Transfer at Fast Flow Rates

When applying Equation 4 to solve for the steady state aqueous mass flux, two limiting cases exist: (i) mass transfer limited and (ii) flow limited. In the mass transfer limited case (i.e., $q>>k_f\alpha$), Equation 4 simplifies to:

$$J \cong qC_s\left(\frac{k_f\alpha L}{q}\right) = C_s k_f \alpha L \qquad [7]$$

Assuming the mass transfer rate coefficient does not vary significantly between gas distributions, a ratio can be used to compare the mass flux between two systems:

$$\frac{J_1}{J_2} \cong \frac{C_s k_f \alpha_1 L}{C_s k_f \alpha_2 L} = \frac{\alpha_1}{\alpha_2} \qquad [8]$$

This ratio was used to compare the mass transfer flux of the heterogeneous discontinuous gas simulations (J_1) and the homogeneous reference simulation (J_2) in their respective 1.1 mm sand compartments under mass transfer limited conditions.

3.3 Flow Limited Mass Transfer at Slow Flow Rates

In the flow limited case (i.e., $q<<k_f\alpha$), Equation 4 simplifies to:

$$J \cong qC_s = \left(\frac{k_{rw}k\rho_w g}{\mu_w}\nabla h\right)C_s \qquad [9]$$

Assuming the intrinsic permeability and hydraulic gradient do not vary significantly between gas distributions, a ratio can be used to compare the mass flux between two systems:

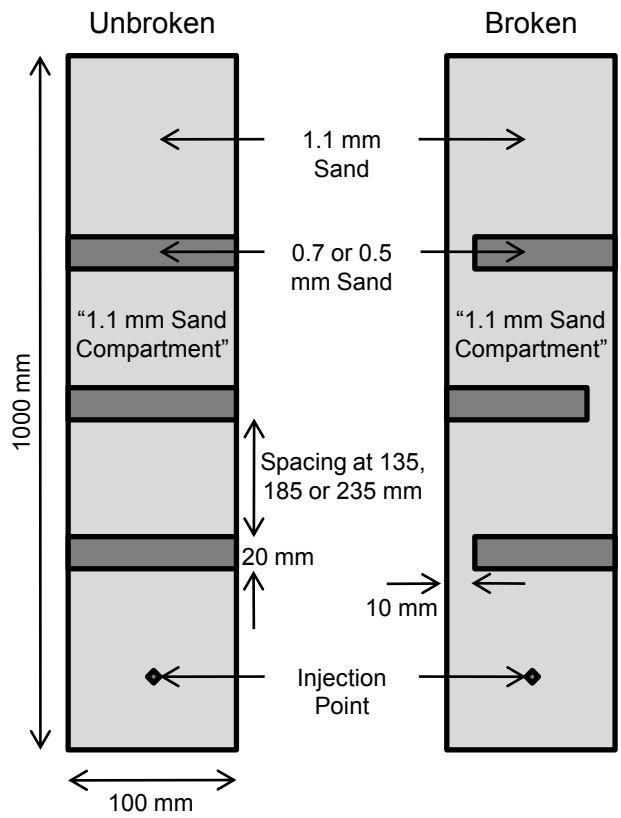

Figure 3: Schematic of the simulation domain showing unbroken and broken capillary barriers.

$$\frac{J_1}{J_2} \cong \frac{q_1 C_s}{q_2 C_s} = \frac{q_1}{q_2} = \frac{k_{rw1}}{k_{rw2}} \quad [10]$$

This ratio was also used to compare the mass flux of the heterogeneous discontinuous gas simulations (J_1) and the homogeneous reference simulation (J_2) in their respective 1.1 mm sand compartments under flow limited conditions.

3.4 Two-Dimensional Interfacial Area Measurements

The two-dimensional interfacial area (α') of the simulated gas clusters was calculated by identifying the number of invaded nodes connected to each non-invaded node. These were then summed to find the total perimeter of the gas clusters in the 1.1 mm sand compartments. It should be noted that the macro-IP model allows two fluids to occupy a single invaded node, and thus a measurement of a simulated gas cluster's perimeter is not the true interfacial area of the system. However, this two-dimensional interfacial area metric was taken to be a representative estimate of the true, effective gas-liquid interfacial area in each simulation.

3.5 Relative Water Permeability

The relative water permeability in the 1.1 mm sand compartments was calculated based on the gas saturation of the compartments. The gas saturation for each row (S_{gj}) in a compartment was calculated as the product of the gas saturation in each grid block (i.e., 0.17) and the fraction of gas-occupied blocks in that row.

A Brooks-Corey Burdine Model was then applied to determine the relative wetting permeability of each row (k_{rwj}):

$$k_{rwj} = \left(S_{ej}\right)^{3+2/\lambda} \quad [11]$$

where S_{ej} is the effective water saturation of row j $\left(S_{ej} = \left[\left(1 - S_{gj}\right) - S_{wr}\right]/(1 - S_{wr})\right)$. The compartment relative permeability (k_{rw}) was estimated as a simple arithmetic average of the relative permeabilities in each row, which is equivalent to assuming that groundwater flow remained parallel to the capillary barriers.

When gases pool behind lenses of lower permeability, gas saturations may be greater in the vicinity of the capillary barrier than the value of 0.17 found during the validation conducted for homogeneous sand packs. To test the sensitivity of the results to the average gas saturation in each block, a value of 0.81 was also used in calculations. This value is the maximum possible gas saturation based on a hydrostatic distribution of gas saturations and the air entry pressures of the media.

4 RESULTS AND DISCUSSION

Figure 4 shows the final gas distributions generated from the macro-IP simulations when capillary barriers are spaced at 185 mm. Similar trends were seen in the 135 mm and 235 mm barrier spacing. The simulated discontinuous gas flow patterns are significantly affected by heterogeneities, causing both pooling behind the unbroken capillary barriers and lateral migration around the broken capillary barriers. This behaviour matches the experimental observations of Glass et al. (2000) and Tomlinson et al. (2003), as discussed previously.

The results from a simulation through 1.1 mm homogeneous sand are shown in Figure 4a. At steady state the discontinuous gas migration path is vertically dominated. During the simulation, injection and fragmentation steps would cause a network of disconnected gas bubbles to repeatedly refill and drain as the network grew vertically; this network is referred to as a discontinuous pipeline. This transient behaviour has also been observed in similar macro-IP models (e.g., Glass and Yarrington 2003).

Figure 4b shows the results from three equally spaced, unbroken 0.7 mm sand capillary barriers in 1.1 mm sand. At steady state, single continuous pools were observed behind each capillary barrier, followed by discontinuous pipelines. During the simulation, it was noted that the discontinuous pipelines behind the pools would become continuous as gas was accumulating behind each pool, and only fragmented again after the gas had broken through the capillary barrier.

Figure 4c shows the results of a simulation similar to Figure 4b, but with unbroken 0.5 mm sand capillary barriers. Simulations with these capillary barriers showed

three regions where different types of behaviour were occurring: single continuous pools behind capillary barriers, fragmented pool transition zones and discontinuous pipelines. The transition zones are continuous as the gas accumulates behind a capillary barrier, and only fragment after the gas breaks through the capillary barrier.

The steady state gas distribution resulting from the broken capillary barrier simulations are shown in Figure 4d. Simulations through the broken capillary barriers produced identical gas distributions when either 0.7 mm sand or 0.5 mm sand capillary barriers were used (at all spacings). This demonstrates that where multiple, short, discontinuous lenses are expected, it is the spacing of the lenses and not their permeability that will control the distribution of discontinuous gas. Although the broken capillary barriers cause lateral migration of the gas, it is expected that given enough horizontal distance to accumulate, the gas may eventually pool enough that it will break through the fine capillary barrier.

Plots of the height of the domain versus the percentage of occupied nodes per row at steady state are shown in Figure 5 for all the simulations. Figure 5b represents the gas distributions illustrated in Figure 4b, 4c and 4d. Since the 0.7 mm and 0.5 mm broken capillary barriers produce the same distribution, they have been combined into a single series on the plots. These plots show the heights of the pools and the transition zones. As expected based on the air entry pressures (Table 1), the simulated pool heights were larger in the presence of the 0.5 mm sand capillary barriers than in the presence of the 0.7 mm sand capillary barriers. Even in cases where gas pooling extended throughout the vertical height of the 1.1 mm sand compartments, the gas saturation was not uniform and aqueous flow through this region is expected.

The average values for the two-dimensional interfacial area and effective relative wetting permeability are shown in Table 2 for the cases where the gas saturation per grid block was taken as 0.17 or 0.81. The mass flux ratios (i.e., Equation 8 for mass transfer limited conditions and Equation 10 for flow limited conditions) are also presented in Table 2. Values presented in Table 2 represent average values from the three 1.1 mm sand compartments in each simulation. Little variation was observed between compartments (Figure 5).

For mass transfer limited conditions it was found that the layered heterogeneities considered here can increase the mass flux behind a capillary barrier above that expected for the homogeneous case. This is due to the increased volume of gas and, consequently, increased interfacial area available for mass transfer despite the existence of more connected gas. The increase was largest for the unbroken 0.5 mm sand capillary barriers, followed by the unbroken 0.7 mm sand capillary barriers, and the broken capillary barriers. The largest increase was 317% and the smallest increase was 44%.

For flow limited conditions, it was found that the layered heterogeneities considered here can decrease the mass flux behind a capillary barrier below that expected for the homogeneous case. This is due to the decrease in relative permeability caused by the increased volume of gas. The change in mass flux was within an order of magnitude for all simulations. Decreases ranged from 3% to 33% assuming a grid-block gas saturation of 0.17, and from 9% to 87% assuming a grid-block gas saturation of 0.81. A comparison of these two limiting case shows that heterogeneity has the potential to either increase or decrease the mass flux from trapped gas in groundwater, depending on the relative rates of interfacial mass transfer and aqueous flow to the gas-occupied region. Under natural groundwater flow conditions, which are expected to be flow limited, a decrease in mass flux is likely, due to decreases in relative permeability. This decrease will be greater where horizontally extensive lenses of finer material are present.

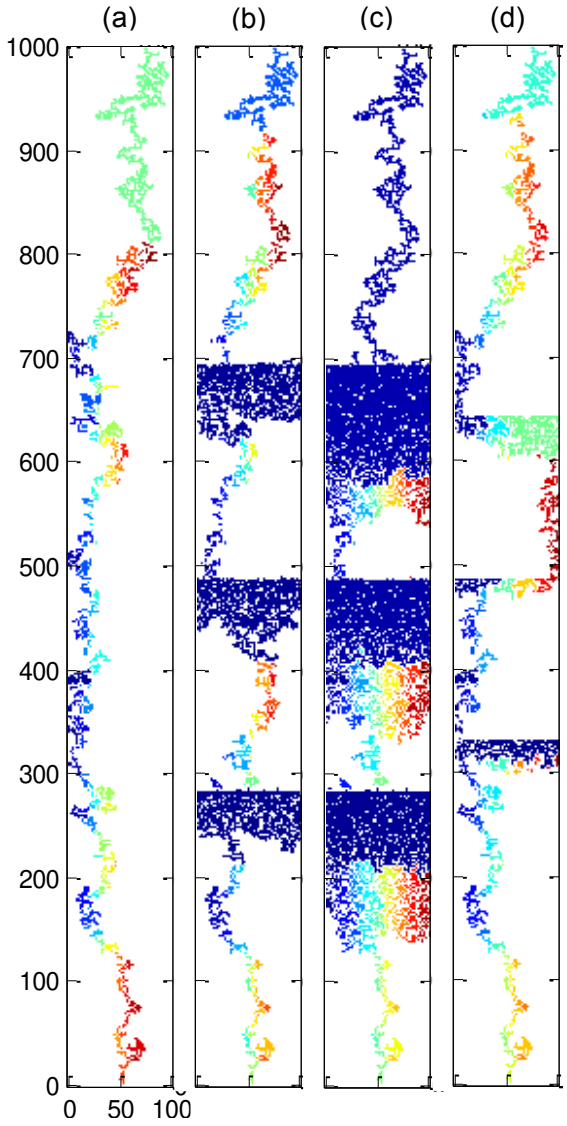

Figure 4: Results for simulations with 185mm of spacing between capillary barriers in (a) homogeneous 1.1mm sand, (b) homogeneous 1.1mm sand with three unbroken 0.7mm capillary barriers, (c) homogeneous 1.1mm sand with three unbroken 0.5mm capillary barriers and (d) homogeneous 1.1 mm sand with three broken 0.7 mm or 0.5 mm capillary barriers.

5 SUMMARY AND CONCLUSIONS

A macroscopic invasion percolation model to simulate discontinuous gas flow in saturated porous media was validated against experimentally-derived saturations in homogeneous sand packs. The model was used to simulate simple heterogeneous systems with both broken and unbroken capillary barriers. As expected, the capillary barriers caused lateral migration and pooling of the discontinuous gas phase, which can increase the interfacial area available for mass transfer and decrease the relative permeability. Under mass transfer limited conditions the potential increase in interfacial area is expected to dominate, which was shown here to increase mass flux from the gas phase. Under flow limited conditions, which likely dominate most groundwater applications, the potential decrease in relative permeability will dominate and will reduce the mass flux from the gas phase compared to a homogeneous case.

These results were found to be sensitive to the spacing, permeability, and lateral extent of the capillary barriers.

Table 2: Summary of the simulated interfacial areas, effective wetting relative permeabilities, and mass transfer ratios.

		Rate Limited		Flow Limited (S_g=0.17)		Flow Limited (S_g=0.81)	
Simulation Type (in 1.1mm Sand)	Capillary Barrier	Average 2D-IFA (α') (mm)	Mass flux ratio (α'_1/α'_2)	Relative Permeability (k_{rw})	Mass flux ratio (k_{rw1}/k_{rw2})	Relative Permeability (k_{rw})	Mass flux ratio (k_{rw1}/k_{rw2})
Spacing = 135 mm							
Homogeneous	None	1033	1.00	0.97	1.00	0.82	1.00
0.7mm Lens	Unbroken	2490	2.41	0.84	0.86	0.51	0.62
0.5mm Lens	Unbroken	4302	4.17	0.65	0.67	0.11	0.13
Both Lenses	Broken	1887	1.83	0.92	0.95	0.76	0.93
Spacing = 185 mm							
Homogeneous	None	1429	1.00	0.97	1.00	0.81	1.00
0.7mm Lens	Unbroken	2848	1.99	0.87	0.90	0.59	0.73
0.5mm Lens	Unbroken	5074	3.55	0.72	0.74	0.26	0.32
Both Lenses	Broken	2287	1.60	0.93	0.96	0.72	0.88
Spacing = 235 mm							
Homogeneous	None	1788	1.00	0.96	1.00	0.82	1.00
0.7mm Lens	Unbroken	3241	1.81	0.88	0.91	0.62	0.76
0.5mm Lens	Unbroken	5000	2.80	0.75	0.78	0.36	0.44
Both Lenses	Broken	2575	1.44	0.94	0.97	0.74	0.91

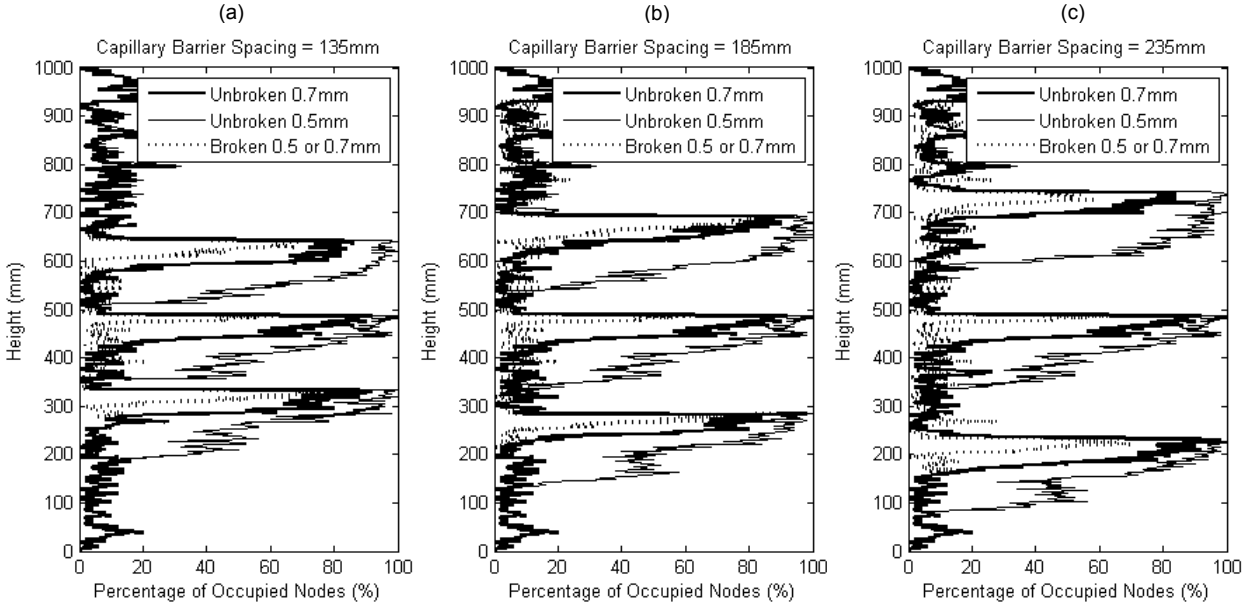

Figure 5: Plots of the height of the domain versus the percentage of occupied nodes per row at steady state for (a) simulations with spacings of 135 mm (b) simulations with spacings of 185 mm and (c) simulations with spacings of 235 mm. The pool transition zones in the 0.5 mm unbroken simulations are the most distinct in the lowest layers.

Accumulation of discontinuous gas into a continuous pool behind capillary barriers should be considered during remediation application. For example, efforts to increase mass transfer rates using pulsed or slowly injected gas intended to produce discontinuous gas bubbles may be undermined by closely-spaced, layered heterogeneities.

ACKNOWLEDGEMENTS

The image processing and validation of the model were funded by an Undergraduate Student Research Award from the Natural Sciences and Engineering Research Council (NSERC) of Canada to P.R. Hegele. We are grateful to M. Rodrigue for translating the abstract to French.

REFERENCES

Brooks, M.C., W.R. Wise, and Annable, M.D. 1999. Fundamental changes in in situ air sparging flow patterns. *Ground Water Monitoring and Remediation*, 19(2): 105–113.

Geistlinger, H., Beckmann., A., and Lazik., D. 2005. Mass transfer between a multicomponent trapped gas phase and a mobile water phase: Experiment and theory. *Water Resources Research*, 41(11): W11408.

Geistlinger, H., Krauss, G., Lazik, D., and Luckner, L. 2006. Direct gas injection into saturated glass beads: Transition from incoherent to coherent gas flow pattern. *Water Resources Research*, 42(7): W07403.

Geistlinger, H., Lazik, D., Krauss, G., and Vogel, H.J. 2009. Pore-scale and continuum modeling of gas flow pattern obtained by high-resolution optical bench-scale experiments. *Water Resources Research,* 45: W04423.

Glass, R.J., Conrad, S.H., and Peplinski, W. 2000. Gravity-destabilized nonwetting phase invasion in macroheterogeneous porous media: experimental observations of invasion dynamics and scale analysis. *Water Resources Research,* 36(11): 3121–37.

Glass, R.J., and Yarrington, L. 2003. Mechanistic modeling of fingering, nonmonotonicity, fragmentation, and pulsation within gravity/buoyant destabilized two-phase/ unsaturated flow. *Water Resources Research*, 39(3): 1058.

Ioannidis, M.A., Chatzis, I., and Dullien, F.A.L. 1996. Macroscopic percolation model of immiscible displacement: Effects of buoyancy and spatial structure. *Water Resources Research*, 32(11): 3297–310.

Johnson, R.L., Johnson, P.C., McWhorter, D.B., Hinchee, R.E., and Goodman, I. 1993. An overview of in situ air sparging. *Ground Water Monitoring and Remediation*, 13(4): 127–135.

Johnson, P.C., Das, A. and Bruce, C. 1999. Effect of flow rate changes and pulsing on the treatment of source zones by in situ air sparging. *Environmental Science Technology*, 33: 1726–1731.

Kueper, B.H., and McWhorter, D.B. 1992. The use of macroscopic percolation theory to construct large-scale capillary pressure curves. *Water Resources Research*, 28(9): 2425–36.

Li, Y., and Wardlaw, N.C. 1986. Mechanisms of nonwetting phase trapping during imbibition at slow rates. *Journal of Colloid and Interface Science*, 109(2): 473–486.

Mumford, K.G., Dickson, S.E., and Smith J.E. 2009. Slow gas expansion in saturated natural porous media by gas injection and partitioning with non-aqueous phase liquids. *Advances in Water Resources*, 32: 29–40.

Mumford, K.G., Smith, J.E., and Dickson, S.E. 2010. The effect of spontaneous gas expansion and mobilization on the aqueous-phase concentrations above a dense non-aqueous phase liquid pool. *Advances in Water Resources,* 33: 504–13.

Niemet, M.R., and Selker, J.S. 2001. A new method for quantification of liquid saturation in 2D translucent porous media systems using light transmission. *Advances in Water Resources*, 24: 651–66.

Powers, S.E., Abriola, L.M., and Weber, W.J. 1992. An experimental investigation of nonaqueous phase liquid dissolution in saturated subsurface systems: steady state mass transfer rates. *Water Resources Research*, 28(10): 2691–2705.

Powers, S.E., Abriola, L.M., Dunkin, J.S., and Weber, W.J. 1994. Phenomenological models for transient NAPL-water mass-transfer processes. *Journal of Contaminant Hydrology*, 16: 1–33.

Reddy, K.R., and Adams, J.A. 2001. Effects of soil heterogeneity on airflow patterns and hydrocarbon removal during in situ air sparging. *Journal of Geotechnical and Geoenvironmental Engineering,* 127(3): 234–247.

Schroth, M.H., Ahearn, S.J., Selker, J.S., and Istok, J.D. 1996. Characterization of miller-similar silica sands for laboratory hydrologic studies. *Soil Science Society of America Journal*, 60(5): 1331–9.

Stöhr, M., and Khalili, A. 2006. Dynamic regimes of buoyancy-affected two-phase flow in unconsolidated porous media. *Physical Review E*, 73: 036301.

Tomlinson, D.W., Thomson, N.R., Johnson, R.L., and Redman, J.D. 2003. Air distribution in the Borden aquifer during in situ air sparging. *Journal of Contaminant Hydrology*, 67: 113–132.

VanAntwerp, D.J., Falta, R.W., and Gierke, J.S. 2008. Numerical Simulation of Field-Scale Contaminant Mass Transfer during Air Sparging. *Vadose Zone Journal*, 7(1): 294-304.

Wagner, G., Birovljev, A., Meakin, P., Feder, J., and Jossang, T. 1997. Fragmentation and migration of invasion percolation clusters: experiments and simulations. *Physical Review E*, 55(6): 7015–29.

Ye, S., Sleep, B.E., and Chien, C. 2009. The impact of methanogenesis on flow and transport in coarse sand. *Journal of Contaminant Hydrology*, 103: 48–57.

Zhao, W., and Ioannidis, M.A. 2011. Gas exsolution and flow during supersaturated water injection in porous media: I. Pore network modeling. *Advances in Water Resources*, 34: 2-14.